The Astrophysical Journal, 960:17 (7pp), 2024 January 1 https://doi.org/10.3847/1538-4357/ad08bc

Sharp Decay of the Internal Plateau in Gamma-Ray Bursts: The Effect of a Cocoon's Thermal Photons on the Jet Emission

Yu-Fei Li, Da-Bin Lin, Jia Ren, Xiao-Yan Li, Guo-Peng Li, and En-Wei Liang
Guangxi Key Laboratory for Relativistic Astrophysics, School of Physical Science and Technology, Guangxi University, Nanning 530004, People's Republic of China; lindabin@gxu.edu.cn
Received 2023 March 28; revised 2023 August 4; accepted 2023 October 31; published 2023 December 19

Abstract

Sub-TeV or TeV γ-rays have been convincingly detected in the afterglows of some gamma-ray bursts (GRBs). The relativistic jet associated with GRBs may be surrounded by a cocoon and thus the thermal photons of the cocoon pervading the emission region of the jet can be upscattered to the very-high-energy regime (e.g., sub-TeV/TeV) by the electrons in the jet. In this scenario, the electrons in the jet cool down and thus the jet emission in the low-energy regime, e.g., the X-ray or optical, may be suppressed. In this paper, we study the effect of the cocoon's thermal photons on the jet emission in the low-energy regime. We find that the jet emission in the low-energy regime is significantly suppressed when the emission region of the jet is just encircled by a hot cocoon. Correspondingly, there is a sharp decay in the light curves of the jet emission in the low-energy regime, which can be understood to signify strong TeV emission in GRBs. Since the radius of the cocoon expands with the observer time $t_{\rm obs}$, the suppression of the jet emission in the low-energy regime may be relieved and thus the light curves of the jet emission would return to those of emission without a cocoon-external inverse-Compton cooling effect. For a long-lasting jet with power $\propto(1+t_{\rm obs}/t_c)^{\alpha}$, an internal plateau followed by a sharp decay may generally appear.

Unified Astronomy Thesaurus concepts: Gamma-ray bursts (629)

1. Introduction

The radiation origin of gamma-ray bursts (GRBs) is still enigmatic in many aspects. While most GRBs are detected below a few MeV, hundreds of cases have been detected above 0.1 GeV and some have been detected even over 10 GeV by Fermi-LAT (Ackermann et al. 2013; Ajello et al. 2019; Noda & Parsons 2022). GRBs have long been believed to be luminous in the GeV–TeV range (e.g., Meszaros & Rees 1994). GRB 180720B was detected by Swift-BAT first and a maximum photon energy of 5 GeV was detected by Fermi-LAT around 142.2 s later (Bissaldi & Racusin 2018). For this burst, the High Energy Stereoscopic System array of telescopes (H.E.S.S.) began observations around 10 hr after the Swift-Burst Alert Telescope (BAT) trigger and a signal strength of 5σ in the energy interval 100–440 GeV was detected (Abdalla et al. 2019). GRB 190114C was identified by Swift-BAT and Fermi-Gamma Burst Monitor (GBM); Hamburg et al. 2019; Krimm et al. 2019). Following the alert from the Swift satellite, the Major Atmospheric Gamma Imaging Cherenkov telescope (MAGIC; Ferenc & MAGIC Collaboration 2005) performed observations on GRB 190114C starting from the first minute to the next 4 hr. Intense sub-TeV/TeV γ-rays were detected from this burst. Besides GRB 180720B and GRB 190114C, GRB 160821B (Acciari et al. 2021), GRB 190829A (H. E. S. S. Collaboration et al. 2021), and GRB 201216C (Fukami et al. 2022) have been reported to emit sub-TeV/TeV γ-rays by H.E.S.S. and/or MAGIC. Recently, GRB 221009A was detected by LHAASO-WCDA at photon energies above 500 GeV with the highest photon energy $\sim$18 TeV, which is the first detection of photons above 10 TeV from GRBs (Huang et al. 2022). A 397.7 GeV photon was also observed by Fermi-LAT for GRB 221009A (Xia et al. 2022).

Many efforts have been made to explain or predict the very-high-energy (VHE) emission in GRBs (e.g., Schneid et al. 1992; Hurley et al. 1994; Katz 1994; Meszaros & Rees 1994; Sommer et al. 1994; Plaga 1995; Schaefer et al. 1998; Beloborodov 2005; Takagi & Kobayashi 2005; Fan et al. 2008; Toma et al. 2009; Kisaka et al. 2015, 2017; Kimura 2019). The synchrotron self-Compton emission (Meszaros & Rees 1994; Dermer et al. 2000; Sari & Esin 2001; Zhang & Mészáros 2001; Ren et al. 2022) or external inverse-Compton (EIC) process (Wang et al. 2006; Ando & Mészáros 2008; Toma et al. 2011; He et al. 2012; Veres & Mészáros 2012; Kimura et al. 2019; Zhang et al. 2021a, 2021b, 2022) within the external shock scenario is usually used to model the VHE emission in these bursts (e.g., GRB 190114C; Asano et al. 2020; Sahu & Fortín 2020; Derishev & Piran 2021; Isravel et al. 2022; Sahu & Valadez Polanco 2022; Sato et al. 2023). It is believed that GRBs are generally formed during the merger of a black hole (BH) and a neutron star (NS)/NS–NS binary (e.g., Paczynski 1986; Meszaros & Rees 1992; Berger 2014; Abbott et al. 2017) or during the collapse of a massive star (e.g., Galama et al. 1998; Hjorth et al. 2003; De Colle et al. 2022). During the merger/collapsar, a hot plasma, i.e., the cocoon, may be formed (Kumar & Smoot 2014). Izzo et al. (2019) reported multi-epoch spectroscopic observations of SN 2017iuk/GRB 171205A and revealed a relativistic thermal cocoon in this catastrophic event. In contrast to the scenario based on the external shock emission used to explain the VHE γ-rays, Kimura et al. (2019) proposed that the cocoon's photons upscattered by nonthermal electrons in the jet may produce a plentiful supply of VHE γ-rays. Correspondingly, this paper is dedicated to studying the effects of the cocoon's thermal photons on the jet emission in the low-energy regime, which may provide information about the strong TeV emission in GRBs.

The paper is organized as follows. The models, i.e., the dynamics of the cocoon and the jet prescription for electron emission, are presented in Section 2. The effects of the cocoon's thermal photons on the jet's emission in the low-energy regime are presented in Section 3. The conclusion and discussion are presented in Section 4.

2. Model

During a merger or collapsar, significant mass is ejected and relativistic jets may be launched from the central engine. The first launched jet makes its way out of the pre-ejected mass or the star along the polar regions. During this process, the material it encounters would be shock-heated and pushed sideways along the jet's direction. Therefore, a cloud of shock-heated plasma surrounding the jet, i.e., a hot cocoon, may form. The cocoon freely expands after it breaks out from the pre-ejected mass or the star. Correspondingly, the emission region of later launched jets may be encircled by the cocoon. In this situation, the thermal photons from the cocoon would pervade the emission region of jets and thus be upscattered to VHE γ-rays (e.g., $\sim$sub-TeV/TeV γ-rays) by nonthermal electrons in the emission region (Kimura et al. 2019). This kind of burst would be an excellent candidate for performing VHE γ-ray surveys. This paper studies the effects of the cocoon's thermal photons on the jet emission in the low-energy regime. We present the dynamics of the cocoon in Section 2.1. The effect of the cocoon's thermal photons on the jet's emission is presented in Section 2.2.

2.1. Dynamics of Cocoon

Dynamics of the cocoon. The dynamics of the cocoon can be obtained based on the evolution of its Lorentz factor $\Gamma_{\rm co}$, internal energy $E'_{\rm co,int}$, volume $V'_{\rm co}$, and radius $R_{\rm co}$ (Kasen & Bildsten 2010; Yu et al. 2013; Sun et al. 2017), i.e.,

$$\frac{d\Gamma_{\rm co}}{dt_{\rm obs}} = \frac{\xi P_{\rm jet} + P_{\rm ra} - L_{\rm co} - \Gamma_{\rm co}\mathcal{D}(dE'_{\rm co,int}/dt')}{M_{\rm co}c^2 + E'_{\rm co,int}}, \quad (1)$$

$$\frac{dE'_{\rm co,int}}{dt_{\rm obs}} = \left[(\xi P'_{\rm jet} + P'_{\rm ra} - L'_{\rm co}) - p'\frac{dV'_{\rm co}}{dt'}\right]\frac{dt'}{dt_{\rm obs}}, \quad (2)$$

$$\frac{dV'_{\rm co}}{dt_{\rm obs}} = 4\pi R_{\rm co}^2\beta_{\rm co}c\frac{dt'}{dt_{\rm obs}}, \quad (3)$$

$$\frac{dR_{\rm co}}{dt_{\rm obs}} = \frac{\beta_{\rm co}c}{1-\beta_{\rm co}}, \quad (4)$$

where a parameter measured in the comoving frame of the cocoon is denoted by a prime, $P_{\rm jet}$ is the jet power, ξ is the fraction of jet power injected into the cocoon, $\mathcal{D} = 1/[\Gamma_{\rm co}(1-\beta_{\rm co})]$ is the Doppler factor, $P_{\rm ra} = P'_{\rm ra}\Gamma_{\rm co}^2$ with $P'_{\rm ra}$ being the radioactive heating rate of the cocoon, $L'_{\rm co} = L_{\rm co}/\Gamma_{\rm co}^2$ with $L_{\rm co}$ being the bolometric luminosity of the cocoon, $M_{\rm co}$ is the mass of the cocoon, $P'_{\rm jet} = P_{\rm jet}/\Gamma_{\rm co}^2$, $p' = E'_{\rm co,int}/(3V'_{\rm co})$ is the pressure of gas in the cocoon, $dt'/dt_{\rm obs} = \mathcal{D}$, and $\beta_{\rm co} = \sqrt{1-1/\Gamma_{\rm co}^2}$. The radiative bolometric luminosity can be related to the internal energy of the cocoon (Kasen & Bildsten 2010; Kotera et al. 2013; Yu et al. 2013) as

$$L'_{\rm co} = \begin{cases} \dfrac{E'_{\rm co,int}c\Gamma_{\rm co}}{\tau R_{\rm co}}, & t_{\rm obs} \leqslant t_{\tau=1}, \\ \dfrac{E'_{\rm co,int}c\Gamma_{\rm co}}{R_{\rm co}}, & t_{\rm obs} > t_{\tau=1}, \end{cases} \quad (5)$$

where $\tau = \kappa(M_{\rm co}/V'_{\rm co})(R_{\rm co}/\Gamma_{\rm co})$ is the optical depth of the cocoon ($\kappa = 0.2\,{\rm cm^2\,g^{-1}}$ is adopted in this paper) and $t_{\tau=1}$ is the observer time at $\tau = 1$.

The radioactive heating rate $P'_{\rm ra}$ would be different if the cocoon is formed in a different scenario. For a cocoon formed in a collapsar, $P'_{\rm ra}$ mainly comes from the decay of radioactive elements ^{56}Ni (Colgate & McKee 1969; Colgate et al. 1980; Arnett 1982) and ^{56}Co (Maeda et al. 2003), i.e.,

$$P'_{\rm ra} = P'_{^{56}{\rm Ni}} \equiv \epsilon_{^{56}{\rm Ni}}M_{^{56}{\rm Ni}}\exp(-t'/T_{^{56}{\rm Ni}}) + \epsilon_{^{56}{\rm Co}}M_{^{56}{\rm Ni}}\frac{\exp(-t'/T_{^{56}{\rm Co}}) - \exp(-t'/\tau_{^{56}{\rm Ni}})}{1-\tau_{^{56}{\rm Ni}}/T_{^{56}{\rm Co}}}, \quad (6)$$

where $\epsilon_{^{56}{\rm Ni}} = 3.9\times10^{10}{\rm erg\,g^{-1}\,s^{-1}}$ is the energy generation rate per unit mass due to ^{56}Ni decay (Sutherland & Wheeler 1984; Cappellaro et al. 1997), $T_{^{56}{\rm Ni}} = 8.8$ days is the e-folding lifetime of ^{56}Ni decay, $\epsilon_{^{56}{\rm Co}} = 6.8\times10^{9}{\rm erg\,g^{-1}\,s^{-1}}$ is the energy generation rate per unit mass due to ^{56}Co decay (Maeda et al. 2003), and $T_{^{56}{\rm Co}} = 111.3$ days is the e-folding lifetime of ^{56}Co decay. The mass of ^{56}Ni can be related to the mass of the cocoon and we take $M_{^{56}{\rm Ni}} = 0.1M_{\rm co}$. For a cocoon formed in a merger, $P'_{\rm ra}$ mainly comes from β-decay (Yu & Li 2017), i.e.,

$$P'_{\rm ra} = P'_{\beta} \equiv 2\times10^{29}M_{\rm co}\times\dot{\epsilon}(t'), \quad (7)$$

with the radioactive power per unit mass (Korobkin et al. 2012; Barnes et al. 2016; Metzger 2017)

$$\dot{\epsilon}(t') = \epsilon_0\left[\frac{1}{2} - \frac{1}{\pi}\arctan\left(\frac{t'-t'_0}{t'_\sigma}\right)\right]^\alpha, \quad (8)$$

where $\epsilon_0 = 2\times10^{18}\,{\rm erg\,g^{-1}\,s^{-1}}$, $\alpha = 1.3$, $t'_0 = 1.3$ s, and $t'_\sigma = 0.11$ s. One should note that the mass of a cocoon formed in a collapsar (e.g., Nakar & Piran 2017; De Colle et al. 2022) may be different from that of a cocoon formed in a merger (e.g., Kimura et al. 2019).

With given values of velocity $\Gamma_{\rm co}$, internal energy $E'_{\rm co,int} = M_{\rm co}(c\beta_{\rm co})^2/2$, volume $V'_{\rm co} = (4/3)\pi R_{\rm co}^3$, and location $R_{\rm co}$ at $t_{\rm obs} = 0$, one can obtain the evolution of $\Gamma_{\rm co}$, $E'_{\rm co,int}$, $V'_{\rm co}$, and $R_{\rm co}$ with respect to $t_{\rm obs}$ for a cocoon. Here, $t_{\rm obs} = 0$ is set at the launch time of the first launched jet from the merger or collapsar. The evolution of $\Gamma_{\rm co}$, $E'_{\rm co,int}$, $V'_{\rm co}$, and $R_{\rm co}$ is numerically calculated with differential Equations (1)–(4), where the fourth-order Runge–Kutta method is employed. In this work, the central engine of the GRB is assumed to be operating in long-duration activity and to thus launch a long-lasting jet. While the first launched jet is making its way out of the pre-ejected mass or the star, the cocoon is formed. Later launched jets would also inject a small fraction of energy into the cocoon during their interaction with it. Therefore, a low value of ξ, e.g., $\xi = 0.01$ (e.g., Yu et al. 2013), is adopted in this paper. Other values of ξ are also tested and are found to affect the dip time of the light curves for the jet emission.

2.2. Jet Prescription and Corresponding Emission

The cocoon freely expands after it breaks out from the pre-ejected mass or the star. Then, the dissipation region of later launched jets may be encircled by the cocoon at a certain time. Here, a long-lasting jet is taken. The cocoon's thermal photons would affect the jet's emission through EIC cooling of the electrons in the jet. In the dissipation region, we assume a fraction $\varepsilon_{\rm dis}$ of the jet power is dissipated. In addition, a fraction $\epsilon_B = 0.01$ of the dissipated energy is used to amplify the magnetic field and a fraction $\epsilon_e = 0.1$ of the total dissipated energy is used to accelerate electrons (Kimura et al. 2019). Thus, the magnetic field strength in the comoving frame of the jet can be described as

$$B''(t_{\rm obs}) = \sqrt{\frac{2\epsilon_B \varepsilon_{\rm dis} P_{\rm jet}(t_{\rm obs})}{R_{\rm dis}^2 \Gamma_{\rm jet}^2 c}}, \quad (9)$$

where parameters measured in the jet comoving frame are denoted by a double prime, $R_{\rm dis}$ is the radius of the dissipation region, and $\Gamma_{\rm jet}$ is the Lorentz factor of the jet at the dissipation region. In this work, $\varepsilon_{\rm dis} = 0.1$ and $\Gamma_{\rm jet} = 200$ (e.g., Yi et al. 2017) are adopted.

In the dissipation region of the jet, the differential electron injection rate is taken as a power-law function with an exponential cutoff (Kimura et al. 2019), i.e., $Q'' = Q''_{\rm nor}(\gamma''_e/\gamma''_m)^{-p}\exp(-\gamma''_e/\gamma''_{e,\rm cut})$ for $\gamma''_e \geqslant \gamma''_m$ and $Q'' = 0$ for $\gamma''_e < \gamma''_m$, where γ''_e is the Lorentz factor of the injected electrons, $\gamma''_{e,\rm cut}$ is the cutoff Lorentz factor, γ''_m is the minimum Lorentz factor of the injected electrons, and a power-law index $p = 2.2$ is adopted (Kimura et al. 2019). The value of $Q''_{\rm nor}$ is obtained by solving $\int_{\gamma''_m}^{+\infty} Q'' d\gamma''_e = P_{\rm jet}/(\Gamma_{\rm jet}^2 m_p c^2)$ and $m_e c^2 \int_{\gamma''_m}^{+\infty} Q''\gamma''_e\, d\gamma''_e = \varepsilon_{\rm dis}\epsilon_e P_{\rm jet}$ together, where c is the velocity of light, and m_p and m_e are the mass of protons and electrons, respectively. Here, $P_{\rm jet}/(\Gamma_{\rm jet}^2 m_p c^2)$ is the total injection rate of electrons in the dissipation region with units of counts per second and $\varepsilon_{\rm dis}\epsilon_e P_{\rm jet}$ is the total power of the injected electrons. Assuming that the electron energy distribution $N''_e(\gamma_e, t_{\rm obs})$ is steady in the dissipation region, the continuity equation of electrons can be written as (Jamil 2011; Kimura et al. 2019)

$$\begin{cases} \frac{\partial}{\partial\gamma''_e}\left(-\frac{\gamma''_e}{t''_{\rm cool}}N''_e\right) = Q, & \gamma''_e \geqslant \min\{\gamma''_m, \gamma''_c\}, \\ N''_e = 0, & \gamma''_e < \min\{\gamma''_m, \gamma''_c\}, \end{cases} \quad (10)$$

where $\gamma''_c = 6\pi m_e c/(t''_{\rm dyn}\sigma_{\rm T}B''^2)$ is the cooling Lorentz factor of electrons in the dissipation region, $\sigma_{\rm T}$ is the Thomson cross section, $t''_{\rm dyn} = R_{\rm dis}/(\Gamma_{\rm jet}c)$ is the dynamic timescale, $t''^{-1}_{\rm cool} = t''^{-1}_{\rm syn} + t''^{-1}_{\rm eic}$, $t''_{\rm syn} = \gamma''_e/\dot{\gamma}''_{e,\rm syn}$, and $t''_{\rm eic} = \gamma''_e/\dot{\gamma}''_{e,\rm eic}$. Here, $m_e c^2\dot{\gamma}''_{e,\rm syn}$ and $m_e c^2\dot{\gamma}''_{e,\rm eic}$ are, respectively, the cooling rate of electrons due to synchrotron emission and EIC emission, i.e.,

$$\dot{\gamma}''_{e,\rm syn}(t_{\rm obs}) = -\frac{3}{2}\frac{\sigma_{\rm T}\gamma''^2_e B''^2}{6\pi m_e c}, \quad (11)$$

$$\dot{\gamma}''_{e,\rm eic}(t_{\rm obs}) = -\frac{1}{m_e c^2}\frac{3\sigma_{\rm T}c}{4\gamma''^2_e}\int_{\nu''_{s,\min}}^{\nu''_{s,\max}}[n''_s(\nu''_s, t_{\rm obs})/\nu''_s]d\nu''_s \times\int_{\nu''_{\rm eic,min}}^{\nu''_{\rm eic,max}} F(q,g)h\nu''_{\rm eic}\, d\nu''_{\rm eic}, \quad (12)$$

where $n''_s(\nu''_s, t_{\rm obs})$ is the number density of seed photons in the jet dissipation region both at frequency ν''_s and at the observer time $t_{\rm obs}$; $F(q, g)$ is a quantity related to the scattering cross section,

$$F(q,g) = \begin{cases} 2q\ln q + (1+2q)(1-q) + \frac{(qg)^2}{2(1+qg)}(1-q), & 0 < q < 1, \\ 0, & q \geqslant 1 \text{ or } q \leqslant 0, \end{cases} \quad (13)$$

with $g = 4\gamma''_e h\nu''_s/(m_e c^2)$ and $q = E/[g(1-E)]$ with $E = h\nu''_{\rm eic}/(\gamma''_e m_e c^2)$; and $h\nu''_{\rm eic,min} = h\nu''_s$ and $h\nu''_{\rm eic,max} = h(\nu''_{\rm eic}/E)[g/(g+1)]$ are the lower and upper limits of the photon energy through the upscattered seed photons $h\nu''_s$, respectively.

When the dissipation region of the long-lasting jet is encircled by the cocoon, the thermal photons from the cocoon would pervade the dissipation region and serve as the seed photons in Equation (12). In this situation, the energy density of seed photons observed in the jet comoving frame can be expressed as (Kimura et al. 2019)

$$U''_s(\nu''_s, t_{\rm obs}) = \Gamma_{\rm jet,co}\frac{8\pi(h\nu''_s/\Gamma_{\rm jet,co})^3}{h^3c^3}\frac{1}{\exp[h\nu''_s/(k_{\rm B}T'_{\rm co}\Gamma_{\rm jet,co})]-1}, \quad (14)$$

where $\Gamma_{\rm jet,co}(t_{\rm obs}) = \Gamma_{\rm jet}\Gamma_{\rm co}(1-\beta_{\rm jet}\beta_{\rm co})$ with $\beta_{\rm jet} = \sqrt{1-1/\Gamma_{\rm jet}^2}$, $T'_{\rm co} = [E'_{\rm co,int}/(aV'_{\rm co})]^{1/4}$ is the temperature of the cocoon observed in the cocoon comoving frame, and $h\nu''_s$ is the energy of seed photons observed in the jet comoving frame. The number density of seed photons in the dissipation region of the jet reads as

$$n''_s(\nu''_s, t_{\rm obs}) = U''_s(\nu''_s, t_{\rm obs})/(h\nu''_s). \quad (15)$$

Jet emission. The synchrotron emission power at a specific frequency $\nu'' = \nu_{\rm obs}/(2\Gamma_{\rm jet})$ in the jet comoving frame can be described as (Sari et al. 1998; Li et al. 2021)

$$f''_{\rm syn}(\nu, t''_{\rm obs}) = \frac{\sqrt{3}\,q_e^3 B''}{m_e c^2}\int_{\gamma''_{e,\min}}^{\gamma''_{e,\max}} N''_e\, F(\nu''/\nu''_{\rm syn})d\gamma''_e, \quad (16)$$

where q_e is the charge of an electron, $F(x) = x\int_x^{+\infty} K_{5/3}(s)ds$ is the modified Bessel function of 5/3 order, and $\nu''_{\rm syn} = 3q_e B''\gamma''^2_e/(4\pi m_e c)$.

The EIC emission power at a specific observed frequency $\nu''_{\rm eic} = \nu_{\rm obs}/(2\Gamma_{\rm jet})$ can be described as (Blumenthal & Gould 1970; Zhang et al. 2019)

$$f''_{\rm eic}(\nu''_{\rm eic}, t_{\rm obs}) = \frac{3\sigma_{\rm T}ch\nu''_{\rm eic}}{4}\int_{\nu''_{s,\min}}^{\nu''_{s,\max}}[n''_s(\nu''_s, t_{\rm obs})/\nu''_s]d\nu''_s \times\int_{\gamma''_{e,\min}}^{\gamma''_{e,\max}}\frac{F(q,g)}{\gamma''^2_e}N''_e\, d\gamma''_e. \quad (17)$$

The observed total flux can be described as

$$F_{\nu_{\rm obs}}(t_{\rm obs}) = \frac{\Gamma_{\rm jet}(f''_{\rm syn} + f''_{\rm eic})(1+z)}{4\pi d_L^2}, \quad (18)$$

where $d_L = 10^{27}$ cm is the luminosity distance of the burst.

3. Results: Effects of the Cocoon on the Jet Emission

Cocoon's properties versus its radius $R_{\rm co}$. When the emission region of a jet is surrounded by a cocoon, the thermal photons from the cocoon would diffuse into the emission region and thus affect the electrons there. In this scenario, the properties of the cocoon, e.g., $k_{\rm B}T'_{\rm co}$, $\Gamma_{\rm co}\beta_{\rm co}$, and $t_{\rm obs}$, relative to its radius $R_{\rm co}$ are important. In Figure 1, we plot the relations

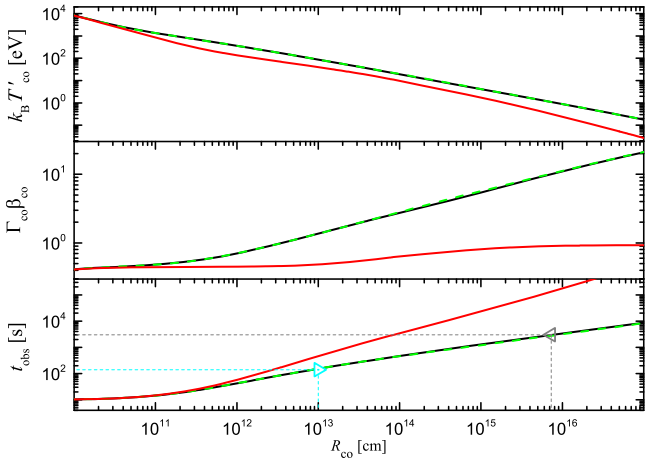

Figure 1. Relations of $k_B T'_{co} - R_{co}$ (upper panel), $\Gamma_{co}\beta_{co}$–R_{co} (middle panel), and t_{obs}–R_{co} (bottom panel) for a fiducial cocoon, where the black solid and green dashed lines are for a cocoon formed during a BH/NS–NS merger and during a massive stellar collapse, respectively. The case with $P_0 = 10^{48}$ erg s^{-1} is also plotted with red solid lines, where other parameters are the same as those for the plotted black solid lines. The open triangle pointing right and the open triangle pointing left correspond to the beginning and end of the sink phase of the green line in Figure 3, respectively.

$k_B T'_{co} - R_{co}$ (upper panel), $\Gamma_{co}\beta_{co}$–R_{co} (middle panel), and t_{obs}–R_{co} (bottom panel) for a cocoon, where the case with $M_{co} = 10^{-4} M_\odot$, $\beta_{co}(t_{obs} = 0) = 0.3$, $R_{co}(t_{obs} = 0) = 3 \times 10^9$ cm, and $P_{jet} = P_0(1 + t_{obs}/t_c)^\alpha$ with $P_0 = 10^{50}$ erg s^{-1}, $t_c = 10^4$ s, and $\alpha = -2$ is adopted as a fiducial example. In this figure, the black solid and green dashed lines are for a cocoon formed during a BH/NS–NS merger and during a massive stellar collapse, respectively. One can find that the black solid and green dashed lines in Figure 1 almost overlap each other. It reveals that the evolution of cocoons formed in different scenarios does not present very large differences if the initial conditions of the cocoons are the same. Therefore, we do not distinguish the formation channel of the cocoon and $P'_{ra} = P'_\beta$ is taken hereafter. The effect of thermal photons on the jet emission is related to the temperature of the cocoon. The upper panel of Figure 1 shows that the $k_B T'_{co}$ of a cocoon decreases significantly as the cocoon expands. In Figure 1, we also plot the case with $P_0 = 10^{48}$ erg s^{-1} (red solid lines), where the values of other parameters are the same as those of the fiducial case. It can be found that the relation $k_B T'_{co} - R_{co}$ does not present very large differences for the case with different P_0. However, the relation $\Gamma_{co}\beta_{co}$–R_{co} and thus the relation t_{obs}–R_{co} are very different. If a higher P_0 is adopted, the cocoon would be accelerated to a high velocity with less time and would thus take less time to reach the same R_{co}. The relation t_{obs}–R_{co} would determine the temperature of the seed (thermal) photons observed by the jet at t_{obs}.

Suppression of the jet emission by the cocoon. The cocoon's thermal photons can be upscattered to VHE γ-rays by nonthermal electrons in the jet (Kimura et al. 2019). Correspondingly, the nonthermal electrons suffer from EIC cooling and thus the jet emission in the low-energy regime may be affected. The electron cooling through the synchrotron emission and that through the EIC emission are proportional to the energy density of the seed photons and the magnetic fields, respectively. In Figure 2, we plot the relation e''_{rad}–R_{co} with a blue dashed line, where $e''_{rad} = aT'^4_{co}\Gamma^2_{jet,co}$ is the energy density of the cocoon's thermal photons observed in the jet comoving frame,

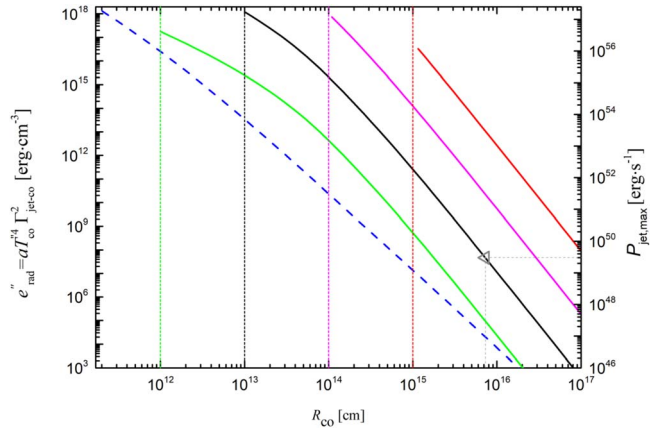

Figure 2. Relations of e''_{rad}–R_{co} (blue dashed line) and –R_{co} for jets with $R_{dis} = 10^{12}$ (green line), 10^{13} (black line), 10^{14} (magenta line), or 10^{15} (red line). The open triangle corresponds to the end of the sink phase in the green line of Figure 3.

$\Gamma_{jet,co} = \Gamma_{jet}\Gamma_{co}(R_{co})[1 - \beta_{jet}\beta_{co}(R_{co})]$, and $\Gamma_{jet} = 200$ (e.g., Yi et al. 2017) is adopted as an example. One can find that the energy density of the cocoon's thermal photons decreases quickly as the cocoon expands. However, the energy density of magnetic fields e''_B in the emission region of the jet is $e''_B = \epsilon_B \varepsilon_{dis} P_{jet}/(4\pi R^2_{dis}\Gamma^2_{jet}c)$, which is mainly related to P_{jet} and R_{dis}. In our scenario, the jet emission can be influenced only if the following two conditions are satisfied: (1) the EIC cooling dominates the electron cooling, i.e., $e''_{rad}\sigma > \sigma_T e''_B$; (2) the emission region of the jet is surrounded by the cocoon, i.e., $R_{dis} < R_{co}$. Here, σ is the photon cross section of electrons considering the Klein–Nishina effect and it can be approximately described as $\sigma \approx \sigma_T[1 + 4kT'_{co}\Gamma_{jet,co}\gamma''_m/(m_e c^2)]^{-2}$. Then, we solve the equation $e''_{rad}\sigma = \sigma_T e''_B$ to obtain P_{jet} (denoted with $P_{jet,max}$), which represents the maximum power of the jet effectively influenced by the EIC cooling. Since e''_{rad} decreases as the cocoon expands, the value of $P_{jet,max}$ would vary correspondingly. We plot the relation $P_{jet,max} - R_{co}$ in Figure 2, where $R_{dis} = 10^{12}$ cm (green line), 10^{13} cm (black line), 10^{14} cm (magenta line), and 10^{15} cm (red line) are adopted. This figure reveals that the EIC cooling is generally strong for a jet surrounded by a cocoon. Taking a jet with $P_{jet} = 10^{48}$ erg s^{-1} and $R_{dis} = 10^{13}$ cm as an example, the EIC cooling generally dominates the electron cooling for a jet with $R_{dis} \sim 10^{13-17}$ cm. In addition, a cocoon located at a small R_{co}, e.g., $R_{co} \lesssim 10^{15}$ cm, would present strong EIC cooling on the electrons for a general jet ($P_{jet} \sim 10^{52}$ erg s^{-1}) observed in the GRB.

Long-term jet behavior. The central engine of a GRB may be prolonged and launch a long-lasting jet. In general, the power of a jet quickly decreases with time in a GRB. The time-dependent jet power can be described as $P_{jet} = P_0(1 + t/t_c)^\alpha$, where t_c describes the decay timescale and α is the decay index. For a jet powered by the magnetic dipole radiation of a magnetized NS, t_c is the spin-down timescale and $\alpha = -2$ ($\alpha = 1$) is adopted for the situation where magnetic dipole (gravitational) radiation dominates the spin-down energy loss of the NS. For a jet powered by the accretion disk formed due to the fallback of material, t_c is related to the fallback timescale and $\alpha = -5/3$ is generally adopted. The cocoon freely expands after it breaks out from the pre-ejected mass or the star. This would lead to the following two results: (1) the emission region of the jet may be encircled by the cocoon at a certain time; (2) the EIC cooling on the jet's electrons may become weak with time as the cocoon

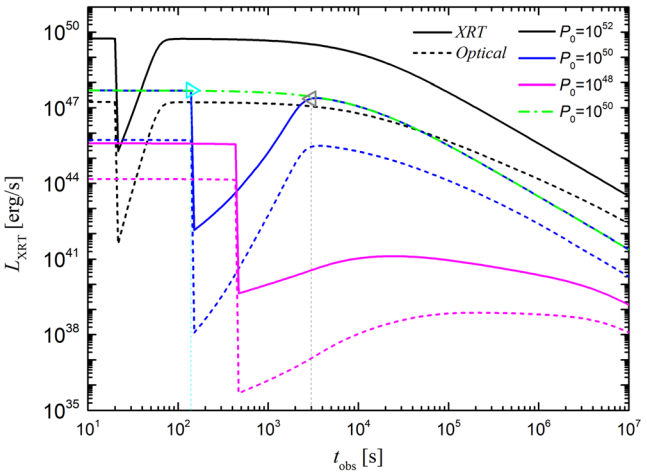

Figure 3. XRT (solid lines) and optical (dashed lines) light curves for the cases with $P_0 = 10^{48}$ (magenta), 10^{50} (blue), and 10^{52} erg s^{-1} (black), where the case without considering the EIC cooling for $P_0 = 10^{50}$ erg s^{-1} is also plotted with a green dashed–dotted line. For the case with $P_0 = 10^{50}$ erg s^{-1}, the open triangle pointing right and the open triangle pointing left are the same as those of Figure 1, indicating the beginning and end of the sink phase, respectively.

expands. The above two behaviors would make an interesting imprint on the light curves of the jet emission. In Figure 3, we plot the light curves of the jet emission in the X-Ray Telescope (XRT) energy band (i.e., 0.3–10 keV, solid lines) and the optical band (i band, dashed lines), where $\alpha = -2$, $t_c = 10^4$ s, and $R_{\rm dis} = 10^{13}$ cm are adopted, and the magenta, blue, and black lines are for the cases with $P_0 = 10^{48}$, 10^{50}, and 10^{52} erg s^{-1}, respectively. For comparison, we also plot the XRT light curves of the jet's emission without considering the EIC cooling (green dashed–dotted line) for the case with $P_0 = 10^{50}$ erg s^{-1}. One can find that a sharp decay followed by a slow recovery phase (dubbed the "sink phase" hereafter) is evident in the XRT/optical light curves for the jet suffering from EIC cooling. By comparing the light curves with and without EIC cooling, one can conclude that the sink phase is formed due to EIC cooling on the electrons. The cocoon's photons are generally upscattered to VHE γ-rays (e.g., $\sim$TeV photons; Kimura et al. 2019), and thus the sink phase that presents in the XRT/optical light curves of the jet emission may signal the strong TeV emission in the corresponding GRB.

The reason for the appearance of the sink phase can be understood as follows. We indicate the beginning and end of the sink phase with cyan open triangle and gray open triangle symbols, respectively. Here, the case with $P_0 = 10^{50}$ erg s^{-1} is discussed. The open triangle pointing right and the open triangle pointing left in Figures 1 and 2 correspond to the beginning and end of the sink phase in Figure 3. (1) Based on the cyan open triangle pointing right in Figure 1, one can find that the beginning of the sink phase is associated with the moment when the cocoon catches up with $R_{\rm dis}$, i.e., $R_{\rm co} = R_{\rm dis}$. This situation, i.e., $R_{\rm co} = R_{\rm dis}$, leads to the sudden increase of seed photons and thus of electron cooling in the emission region of the jet. Correspondingly, the jet emission in the low-energy regime would be suppressed and a sharp decay appears in its light curves. The suppression of the jet synchrotron emission (or the jet emission in the low-energy regime) can be roughly estimated with the value of $\sigma_{\rm T} e''_B/(\sigma e''_{\rm rad} + \sigma_{\rm T} e''_B)$ or $P_{\rm jet}/(P_{\rm jet,max} + P_{\rm jet})$. Taking the case with $P_0 = 10^{50}$ erg s^{-1} as an example, the values of $P_{\rm jet}$ and $P_{\rm jet,max}$ are 9.7×10^{49} erg s^{-1} and 1.5×10^{56} erg s^{-1} at the bottom of the sink phase, respectively. Then, the suppression of the jet synchrotron emission is around 10^6, which is consistent with that in the sink phase, i.e., $\sim 10^5$. The difference between these two suppression factors (i.e., 10^6 versus $\sim 10^5$) reveals that the EIC emission makes a significant contribution to the jet emission in the low-energy regime. (2) The recovery phase of the sink phase would be related to the weakening of the EIC cooling on electrons in the jet's emission region. Based on Figure 2, the maximum power of jets effectively influenced by EIC cooling at the end of the sink phase is $P_{\rm jet,max} \approx 3 \times 10^{49}$ erg s^{-1} (see gray open triangle). The jet power at the end time of the sink phase is estimated to be $P_{\rm jet} \approx 6 \times 10^{49}$ erg s^{-1}, which is around $2P_{\rm jet,max}$. It reveals that the end of the sink phase is related to the moment when the EIC cooling no longer dominates the electron cooling in the jet's emission region. It is worth pointing out that the light curve of the sink phase in the case with low jet power, e.g., $P_0 = 10^{48}$ erg s^{-1}, is very similar to the light curve of an external forward shock with an energy injection phase.

4. Summary and Discussion

In a merger or collapsar, a cocoon may form as the first launched jet makes its way out of the pre-ejected mass or the star. We study the effect of a cocoon's thermal photons on the jet emission, of which the region is surrounded by the cocoon. It is found that EIC cooling generally dominates the electron cooling in the jet. Then, the synchrotron emission of jets in GRBs would be generally suppressed if their emission region is encircled by the cocoon. In a burst, the cocoon freely expands after it breaks out of the pre-ejected mass or the star. The cocoon would catch up with the emission region of a long-lasting jet at a certain time. It leads to the sudden increase of seed photons and thus of electron cooling in the emission region of the jet at that time. Correspondingly, the jet emission in the low-energy regime is suppressed and thus a sharp decay appears in the light curve. Since the temperature of the cocoon decreases as the cocoon expands, the EIC cooling on electrons is weakened with time. Correspondingly, the light curve of jet emission in the low-energy regime may gradually return to that without EIC cooling. In our numerical calculations, a sink phase, i.e., a sharp decay followed by a recovery phase, is indeed present in the light curves of jet emission in the low-energy regime. Since the cocoon's photons are generally upscattered to VHE γ-rays (e.g., $\sim$TeV photons; Kimura et al. 2019), the sink phase that presents in the XRT light curve of jet emission, especially the sharp decay behavior, may signal the strong TeV emission in the corresponding GRB.

The observations of Swift have revealed a mysterious X-ray plateau followed by a sharp decay in some GRBs (Troja et al. 2007; Rowlinson et al. 2010, 2013). This feature, known as the internal plateau, is believed to form during the internal dissipation of the jet. Generally, a long-lived magnetized NS that later collapses into a BH is proposed to explain the internal plateau (Bucciantini et al. 2007, 2008; Bucciantini 2009; Metzger et al. 2011). The sink phase found in this paper may provide another explanation for the sharp decay of the internal plateau, rather than involving the collapse of a magnetized NS. That is to say, the sharp decay of the internal plateau may be due to the strong EIC cooling of electrons in this phase. Taking GRB 070110 as an example, we plot the XRT light curve (solid red line) of emission for a jet surrounded by a cocoon in Figure 4. In this figure, the XRT

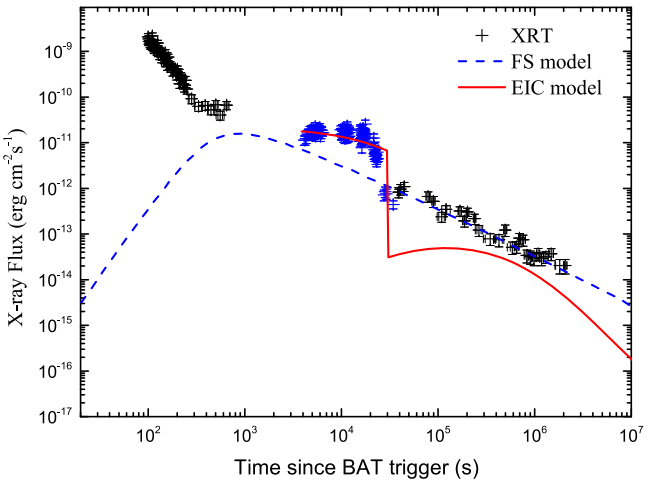

Figure 4. Demonstration of our scenario explaining the steep decay of an internal plateau, where the XRT observational data from the Swift satellite is plotted with plus signs, the blue plus signs indicate the phase of the internal plateau, the red solid line is the XRT light curve of jet emission in our scenario, and the blue dashed line is the XRT emission from the standard external forward shock of Du et al. (2016) for GRB 070110.

observational data from the Swift satellite is plotted with plus signs, and the blue plus signs indicate the phase of the internal plateau. Here, the XRT emission is assumed from a long-lasting jet with $P_0 = 3.0 \times 10^{50}$ erg s^{-1}, $\alpha = -2$, and $t_c \sim 4.0 \times 10^4$ s, where the values of the other parameters are $\gamma_m = 100$, $R_{dis} = 10^{15}$ cm, $\epsilon_B = 0.1$, $\Gamma_{jet} = 100$, $\xi = 10^{-5}$, $M_{co} = 10^{-4} M_\odot$, $\beta_{co}(t_{obs} = 0) = 0.3$, and $R_{co}(t_{obs} = 0) = 3.0 \times 10^9$ cm. One can find that a sharp decay naturally presents in the XRT light curve of jet emission at $t_{obs} \sim 2.0 \times 10^4$ s, which is very similar to that found in GRB 070110 (Krimm et al. 2007; Sbarufatti et al. 2007; Troja et al. 2007; Rowlinson et al. 2010). It should be noted that our scenario is proposed to explain the sharp decay of the internal plateau rather than of the whole afterglow in GRB 070110. Du et al. (2016) proposed that the XRT and optical emission after the steep decay in GRB 070110 is from the standard external forward shock in this burst. To demonstrate, we plot the XRT emission of the standard external forward shock in this burst in Figure 4. Besides, the shallow decay (i.e., the external plateau) followed by a normal decay generally observed in the afterglow of GRBs is always ascribed to an external forward shock with an energy injection phase. However, the straightforward emission of jets responsible for the energy injection phase is always not found in observations. This can be understood if the suppression of jet emission due to EIC cooling works. Correspondingly, one may expect strong VHE γ-rays at around the energy injection phase.

Acknowledgments

This work is supported by the National Natural Science Foundation of China (grant Nos. 12273005 and 12133003), the Guangxi Science Foundation (grant No. 2018GXNSFFA281010), and the China Manned Spaced Project (CMS-CSST-2021-B11).

ORCID iDs

Yu-Fei Li https://orcid.org/0009-0006-2841-678X
Da-Bin Lin https://orcid.org/0000-0003-1474-293X
Jia Ren https://orcid.org/0000-0002-9037-8642
Guo-Peng Li https://orcid.org/0000-0003-3306-5217
En-Wei Liang https://orcid.org/0000-0002-7044-733X

References

Abbott, B. P., Abbott, R., Abbott, T. D., et al. 2017, ApJL, 848, L12
Abdalla, H., Adam, R., Aharonian, F., et al. 2019, Natur, 575, 464
Acciari, V. A., Ansoldi, S., Antonelli, L. A., et al. 2021, ApJ, 908, 90
Ackermann, M., Ajello, M., Asano, K., et al. 2013, ApJS, 209, 11
Ajello, M., Arimoto, M., Axelsson, M., et al. 2019, ApJ, 878, 52
Ando, S., & Mészáros, P. 2008, ApJ, 689, 351
Arnett, W. D. 1982, ApJ, 253, 785
Asano, K., Murase, K., & Toma, K. 2020, ApJ, 905, 105
Barnes, J., Kasen, D., Wu, M.-R., & Martínez-Pinedo, G. 2016, ApJ, 829, 110
Beloborodov, A. M. 2005, ApJL, 618, L13
Berger, E. 2014, ARA&A, 52, 43
Bissaldi, E., & Racusin, J. L. 2018, GCN, 22980
Blumenthal, G. R., & Gould, R. J. 1970, RvMP, 42, 237
Bucciantini, N. 2009, in ASP Conf. Ser. 406, Numerical Modeling of Space Plasma Flows: ASTRONUM-2008, ed. N. V. Pogorelov et al. (San Francisco, CA: ASP), 73
Bucciantini, N., Quataert, E., Arons, J., Metzger, B. D., & Thompson, T. A. 2007, MNRAS, 380, 1541
Bucciantini, N., Quataert, E., Arons, J., Metzger, B. D., & Thompson, T. A. 2008, MNRAS, 383, L25
Cappellaro, E., Mazzali, P. A., Benetti, S., et al. 1997, A&A, 328, 203
Colgate, S. A., & McKee, C. 1969, ApJ, 157, 623
Colgate, S. A., Petschek, A. G., & Kriese, J. T. 1980, ApJL, 237, L81
De Colle, F., Kumar, P., & Hoeflich, P. 2022, MNRAS, 512, 3627
Derishev, E., & Piran, T. 2021, ApJ, 923, 135
Dermer, C. D., Chiang, J., & Mitman, K. E. 2000, ApJ, 537, 785
Du, S., Lü, H.-J., Zhong, S.-Q., & Liang, E.-W. 2016, MNRAS, 462, 2990
Fan, Y.-Z., Piran, T., Narayan, R., & Wei, D.-M. 2008, MNRAS, 384, 1483
Ferenc, D. & MAGIC Collaboration 2005, NIMPA, 553, 274
Fukami, S., Berti, A., Loporchio, S., et al. 2022, ICRC (Berlin), 395, 788
Galama, T. J., Vreeswijk, P. M., van Paradijs, J., et al. 1998, Natur, 395, 670
Hamburg, R., Veres, P., Meegan, C., et al. 2019, GCN, 23707
He, H.-N., Zhang, B.-B., Wang, X.-Y., Li, Z., & Mészáros, P. 2012, ApJ, 753, 178
H. E. S. S. Collaboration, Abdalla, H., Aharonian, F., et al. 2021, Sci, 372, 1081
Hjorth, J., Sollerman, J., Møller, P., et al. 2003, Natur, 423, 847
Huang, Y., Hu, S., Chen, S., et al. 2022, GCN, 32677
Hurley, K., Dingus, B. L., Mukherjee, R., et al. 1994, Natur, 372, 652
Isravel, H., Pe'er, A., & Begue, D. 2023, ApJ, 955, 70
Izzo, L., de Ugarte Postigo, A., Maeda, K., et al. 2019, Natur, 565, 324
Jamil, M. 2011, ConPh, 52, 378
Kasen, D., & Bildsten, L. 2010, ApJ, 717, 245
Katz, J. I. 1994, ApJL, 432, L27
Kimura, S. S. 2019, in EPJ Web of Conferences, Ultra High Energy Cosmic Rays 2018, 210, ed. I. Lhenry-Yvon et al. (EDP Sciences), 03001
Kimura, S. S., Murase, K., Ioka, K., et al. 2019, ApJL, 887, L16
Kisaka, S., Ioka, K., & Nakamura, T. 2015, ApJL, 809, L8
Kisaka, S., Ioka, K., & Sakamoto, T. 2017, ApJ, 846, 142
Korobkin, O., Rosswog, S., Arcones, A., & Winteler, C. 2012, MNRAS, 426, 1940
Kotera, K., Phinney, E. S., & Olinto, A. V. 2013, MNRAS, 432, 3228
Krimm, H. A., Barthelmy, S. D., Cummings, J. R., et al. 2019, GCN, 23724
Krimm, H. A., Boyd, P., Mangano, V., et al. 2007, GCN, 6014
Kumar, P., & Smoot, G. F. 2014, MNRAS, 445, 528
Li, X.-Y., Lin, D.-B., Ren, J., et al. 2021, ApJ, 922, 22
Maeda, K., Mazzali, P. A., Deng, J., et al. 2003, ApJ, 593, 931
Meszaros, P., & Rees, M. J. 1992, ApJ, 397, 570
Meszaros, P., & Rees, M. J. 1994, MNRAS, 269, L41
Metzger, B. D. 2017, LRR, 20, 3
Metzger, B. D., Giannios, D., Thompson, T. A., Bucciantini, N., & Quataert, E. 2011, MNRAS, 413, 2031
Nakar, E., & Piran, T. 2017, ApJ, 834, 28
Noda, K., & Parsons, R. D. 2022, Galax, 10, 7
Paczynski, B. 1986, ApJL, 308, L43
Plaga, R. 1995, Natur, 374, 430
Ren, J., Wang, Y., & Zhang, L.-L. 2023, ApJ, 947, 53
Rowlinson, A., O'Brien, P. T., Metzger, B. D., Tanvir, N. R., & Levan, A. J. 2013, MNRAS, 430, 1061
Rowlinson, A., O'Brien, P. T., Tanvir, N. R., et al. 2010, MNRAS, 409, 531
Sahu, S., & Fortín, C. E. L. 2020, ApJL, 895, L41
Sahu, S., Valadez Polanco, I. A., & Rajpoot, S. 2022, ApJ, 929, 70
Sari, R., & Esin, A. A. 2001, ApJ, 548, 787
Sari, R., Piran, T., & Narayan, R. 1998, ApJL, 497, L17

Sato, Y., Obayashi, K., Theodre Zhang, B., et al. 2023, JHEAp, 37, 51
Sbarufatti, B., Mangano, V., Mineo, T., Cusumano, G., & Krimm, H. 2007, GCN, 6008
Schaefer, B. E., Palmer, D., Dingus, B. L., et al. 1998, ApJ, 492, 696
Schneid, E. J., Bertsch, D. L., Fichtel, C. E., et al. 1992, A&A, 255, L13
Sommer, M., Bertsch, D. L., Dingus, B. L., et al. 1994, ApJL, 422, L63
Sun, H., Zhang, B., & Gao, H. 2017, ApJ, 835, 7
Sutherland, P. G., & Wheeler, J. C. 1984, ApJ, 280, 282
Takagi, R., & Kobayashi, S. 2005, ApJL, 622, L25
Toma, K., Wu, X.-F., & Mészáros, P. 2009, ApJ, 707, 1404
Toma, K., Wu, X. F., & Mészáros, P. 2011, MNRAS, 415, 1663
Troja, E., Cusumano, G., O'Brien, P. T., et al. 2007, ApJ, 665, 599
Veres, P., & Mészáros, P. 2012, ApJ, 755, 12
Wang, X.-Y., Li, Z., & Mészáros, P. 2006, ApJL, 641, L89
Xia, Z.-Q., Wang, Y., Yuan, Q., & Fan, Y.-Z. 2022, GCN, 32748
Yi, S.-X., Lei, W.-H., Zhang, B., et al. 2017, JHEAp, 13, 1
Yu, Y.-W., & Li, S.-Z. 2017, MNRAS, 470, 197
Yu, Y.-W., Zhang, B., & Gao, H. 2013, ApJL, 776, L40
Zhang, B., & Mészáros, P. 2001, ApJ, 559, 110
Zhang, B. T., Murase, K., Ioka, K., et al. 2023, ApJL, 947, L14
Zhang, B. T., Murase, K., Veres, P., & Mészáros, P. 2021a, ApJ, 920, 55
Zhang, B. T., Murase, K., Yuan, C., Kimura, S. S., & Mészáros, P. 2021b, ApJL, 908, L36
Zhang, Y., Geng, J.-J., & Huang, Y.-F. 2019, ApJ, 877, 89